

Limit shapes from harmonicity: dominos and the five vertex model

Richard Kenyon* István Prause†

Abstract

We discuss how to construct limit shapes for the domino tiling model (square lattice dimer model) and 5-vertex model, in appropriate polygonal domains. Our methods are based on the harmonic extension method of [R. Kenyon and I. Prause, Gradient variational problems in \mathbb{R}^2 , Duke Math J. 2022].

1 Introduction

For a convex function $\sigma : \mathbb{R}^2 \rightarrow \mathbb{R} \cup \{\infty\}$, called the *surface tension*, the associated *gradient variational problem* is the problem of minimizing the surface tension integral for functions $h : U \rightarrow \mathbb{R}$ on a domain $U \subset \mathbb{R}^2$

$$\min_h \iint_U \sigma(\nabla h(x, y)) \, dx \, dy, \quad h|_{\partial U} = h_0. \quad (1)$$

In other words this is the problem of finding a function $h : U \rightarrow \mathbb{R}$ with prescribed boundary values $h|_{\partial U} = h_0$ and minimizing the surface tension integral.

Well-known examples of gradient variational problems are the Dirichlet problem for the Laplacian, where $\sigma(\nabla f) = |\nabla f|^2$, and the minimal surface equation, where $\sigma(\nabla f) = \sqrt{1 + |\nabla f|^2}$.

In statistical mechanics, many *limit shape problems* are gradient variational problems, for example the limit shapes for dimers [7] and the five- and six-vertex models [8, 16].

In [15] we showed that any gradient variational problem (1) can be reduced to a harmonic extension problem: any surface tension minimizer is the envelope of a family

*Department of Mathematics, Yale University, New Haven CT 06520; richard.kenyon at yale.edu. Research supported by NSF DMS-1940932 and the Simons Foundation grant 327929.

†Department of Physics and Mathematics, University of Eastern Finland, P.O. Box 111, 80101 Joensuu, Finland; istvan.prause at uef.fi. Research supported by Academy of Finland grant 355839 and Väisälä foundation travel grant.

2010 *Mathematics Subject Classification*: Primary 49Q10, 35C99; Secondary 82B20.

of planes in \mathbb{R}^3 whose defining coefficients are κ -harmonic functions of the intrinsic (isothermal) coordinate z . Here κ is the square root of the determinant of the Hessian $\text{Hess}(\sigma)$ with respect to the intrinsic coordinate; by κ -harmonic function we mean a function $f : \Omega \rightarrow \mathbb{R}$, $\Omega \subset \mathbb{R}^2$ satisfying

$$\nabla \cdot \kappa \nabla f = 0. \tag{2}$$

This is called the inhomogeneous-conductance Laplace equation [3], and is the analog of a harmonic function in the presence of a varying positive conductance field $\kappa = \kappa(x, y)$.

In the current paper we apply this procedure to get explicit limit shapes for two particular statistical mechanics models: the square grid dimer model (domino tiling model) and 5-vertex model.

Limit shapes for the dimer model were originally discussed by Cohn, Kenyon and Propp in [7] and Kenyon and Okounkov in [12]. See also more recent work by Astala, Duse, Prause, and Zhong in [2], where general results are obtained about geometry and regularity of limit shapes. An explicit construction for limit shapes was given for a particular dimer model, the honeycomb dimer model, in [12]. This is, in a well-defined sense, the simplest dimer model. Extending the ideas of [12] to other dimer models such as the square grid dimer model, however, has been problematic until recently, primarily due to two difficulties: higher degree spectral curves and the problem of “matching parameters”. The work [2] does apply to higher degree spectral curves and indeed for quite general dimer models but it is of limited value in finding a limit shape matching a given set of boundary conditions. Using the recently developed method of [15] of harmonic extension we can now carry out this matching procedure for a larger class of dimer models: the so-called isoradial, or genus-zero cases (which include the domino cases). Note that the recent work [4] solves the limit shape problem for more general higher genus dimer models but only for a specific domain, the “Aztec diamond”. For comparison, we illustrate our method on a genus one example in Section 2.3.

The dimer model has the special feature that κ of equation (2) is constant, so κ -harmonic functions are simply harmonic functions. Moreover for the standard polygonal domains (defined below), we have *a priori* knowledge about the tangent planes to the limit shapes along ∂U , so the corresponding harmonic extension problem can be quite explicitly carried out. This is explained in Section 2 below, and an explicit worked example is given.

The 5-vertex model is a generalization of the dimer model for which κ is not constant; nonetheless it has a special property, called the “trivial potential” property [15], that $\sqrt{\kappa}$ is a harmonic function of the intrinsic coordinate z . This implies [15] that a κ -harmonic function is the ratio of a harmonic function and a certain fixed function $\theta = \theta(z)$. This fact allows us to likewise give an essentially complete limit shape theory for the five-vertex model, again for the appropriate polygonal domains.

We show in the last section, Section 4, that the 4-vertex model of [6] also has trivial potential, and in fact its limit shapes are obtained from the lozenge dimer model limit shapes by a linear transformation.

We should mention here that limit shapes for most of the basic statistical mechanical models are not known, even for the six-vertex model. To find limit shapes one needs an

explicit expression for the surface tension, or free energy, for general parameters, and this is not usually available, especially for “non-free fermionic” models. The method presented in this paper applies in principle also for the six-vertex model, replacing harmonic functions with κ -harmonic functions. The key difficulty is that κ is not known in this case. Finally, we should mention the effect of κ on fluctuations: we expect these to be described by an *inhomogeneous* Gaussian free field, see [5], associated to the κ -Laplacian operator of (2) in the intrinsic complex structure given by the z -coordinate.

2 Domino limit shapes

See [11] for background on domino tilings and dimers in general. We discuss here the square grid dimer model, or domino tiling model. This material can be easily extended to the case of general periodic isoradial dimers (defined in [10]), however for simplicity of notation we deal with only the domino case here.

The features of the domino model we need for the current discussion are the following.

1. Let $N = [0, 1]^2$, the “Newton polygon” (see [13]). The surface tension $\sigma = \sigma(s, t)$ of (1) is analytic on N , $+\infty$ outside of N , and strictly convex on the interior of N (the so-called *rough phase*, or *liquid phase*). Thus our minimizers h have gradient $\nabla h = (s, t)$ constrained to lie in N .
2. The Hessian of σ defines on N a Riemannian metric [15]. The intrinsic coordinate z (the conformal coordinate) for this metric can and will be chosen to be parameterized by the upper half plane: $z \in \mathbb{H}$. There is another intrinsic coordinate w , where $w \in \bar{\mathbb{H}}$, the lower half plane, related to z through the “spectral curve” $P(z, w) = 1 + z + w - zw = 0$. See Figure 1.
3. For $(s, t) \in N$ the relation between s, t and z is

$$(s, t) = \frac{1}{\pi}(\pi - \arg z, \pi + \arg w). \quad (3)$$

See Figure 1.

We orient edges of N counterclockwise, and label them cyclically 1, 2, 3, 4 with 1 being the lower edge. Let $R_0 \subset \mathbb{R}^2$ be a polygon with $4n$ sides, with edges orthogonal to those of N , and occurring in *clockwise* order around the boundary. That is, edges of R_0 are oriented clockwise around R_0 and are labelled 1, 2, 3, 4 cyclically: 1, 2, 3, 4, 1, 2, 3, 4, \dots , with edges of label i associated to, and orthogonal to, edge i of N . See Figure 2 for an example. Generally we can allow some edges of R_0 to have length 0.

Let $\mathcal{G} = e^{i\pi/4}\mathbb{Z}^2$, the square grid rotated by $\pi/4$. We consider dimer covers of regions $R = R_\varepsilon$ in $\varepsilon\mathcal{G}$, approximating R_0 as $\varepsilon \rightarrow 0$, such that edges of R consist of zig-zag paths of $\varepsilon\mathcal{G}$ as in Figure 2. For example a “vertical boundary” of R of type 3 corresponds to an alternating sequence of NW- and NE-edges of \mathcal{G} . An edge of R of type 1 is vertical and either oriented upwards or downwards (when moving clockwise

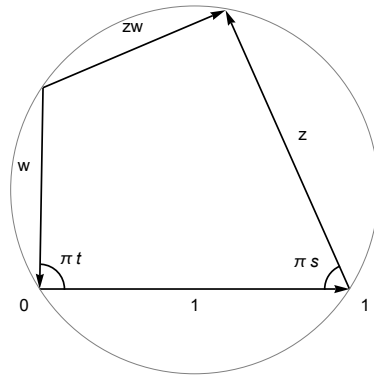


Figure 1: Relation between z, w, s, t for dominos. Given $z \in \mathbb{H}$, draw a circle passing through $0, 1$ and $1 + z$. Then w, s, t are determined as shown.

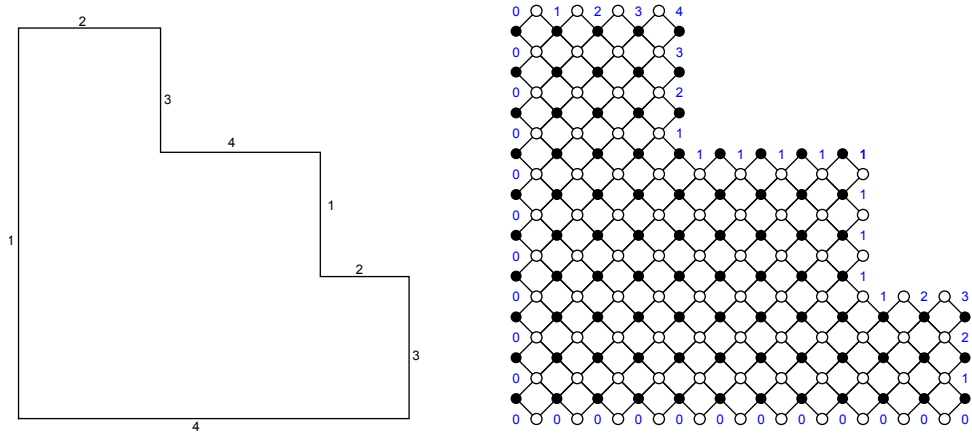


Figure 2: Polygon R_0 and approximating graph \mathcal{G} with boundary height function (in blue).

around R); if upwards it has black vertices on the outside and if downwards it has white vertices on the outer side of R , as in Figure 2. Similar conditions hold for the other types of edges. To each corner of R is associated a vertex of N .

The height function¹ on the boundary of R is defined on faces along the boundary, is constant on edges of types 1 and 4, and increasing rightwards on edges of type 2 and upwards on edges of type 3, again as in Figure 2. The fact that the height function is well-defined around the boundary is a necessary condition for existence of a dimer cover (it implies that the graph is balanced, that is, has the same number of white vertices as black vertices). The condition of being balanced is a linear condition on the signed sidelengths: the total signed length of edges of type 2 equals the total signed length of edges of type 3 (where we define the length of these edges to be the number of vertices along them, not including vertices at concave corners).

Suppose R_0 is as above, and let R be the associated approximating region in $\varepsilon\mathcal{G}$. We translate R_0 and R so that $(0, 0)$ is at a convex corner of R_0 , with sides $1, 2, \dots, 4n$ in clockwise order starting from $(0, 0)$. We orient R and R_0 so that side 1 is vertical upwards, of type 1, and side $4n$ is horizontal leftwards (of type 4). The slopes of the height function of a dimer cover of R near the vertices of R , ordered clockwise, run consecutively counterclockwise around the vertices of N , and are periodic with period 4:

$$(0, 0), (1, 0), (1, 1), (0, 1), (0, 0), \dots$$

Letting L_i be the signed length of side i of R_0 , the tangent planes to the limit shape in R_0 near the corners of R_0 are determined by these slopes and heights:

$$0, x, x + y - L_1, x + L_2 - L_1, L_2 - L_3, \dots$$

The rough phase region in the limit shape (the region where the gradient lies in the interior of N) is parameterized by $u \in \mathbb{H}$; the diffeomorphism from the rough phase region to $u \in \mathbb{H}$ *reverses orientation* (this is just conventional; we could instead parameterize the rough phase region with the lower half-plane, and then orientation would be preserved). Here u is an n -fold cover of $z \in \mathbb{H}$, that is, $z = z(u)$ is a rational function of degree n . We let $a_1, a_2, \dots, a_{4n} \in \hat{\mathbb{R}}$ be the points u , in reverse order around $\hat{\mathbb{R}}$, at which the rough phase region is tangent to the (extended) lines corresponding to the sides of R_0 . These are points at which z takes value $\{-1, 0, 1, \infty, -1, 0, 1, \infty, \dots\}$. Thus z necessarily has the form

$$z = B_1 \frac{(u - a_2)(u - a_6) \dots (u - a_{4n-2})}{(u - a_4)(u - a_8) \dots (u - a_{4n})}$$

for a constant B_1 . Likewise we have

$$w = \frac{B_2(u - a_1)(u - a_5) \dots (u - a_{4n-3})}{(u - a_3)(u - a_7) \dots (u - a_{4n-1})}.$$

¹This version of the height function is defined by comparing a dimer cover m of R with the fixed dimer cover m_0 of \mathcal{G} which uses all dimers on \mathcal{G} which are oriented NW/SE with black NW vertex. The union $m \cup m_0$ consists in doubled edges and oriented chains of dimers, which are oriented so that dimers from m_0 are oriented from black to white. The height, defined on the faces of R , is constant on complementary components of the chains and increases by one when crossing a chain oriented from left to right. See [11].

From $P(z, w) = 0$ we have $w = \frac{z+1}{z-1}$ which can be used to determine $B_2, a_1, a_3, \dots, a_{4n-1}$ as functions of $B_1, a_2, a_4, \dots, a_{4n}$.

The equation

$$s_u x + t_u y + c_u = 0 \tag{4}$$

parameterizes the tangent lines to the arctic curve as u runs over $\hat{\mathbb{R}}$, see [14]. The roots of s_u therefore correspond to the horizontal sides of R , the roots of t_u correspond to the vertical lines of R , and the roots of c_u are the tangent lines through the origin.

There is one extra necessary condition on the a_i , which is that we need c_u to vanish at the critical points of $z = z(u)$:

Lemma 2.1. *The quantity c_u vanishes at the critical points of $z(u)$. At higher order critical points c_u vanishes with the corresponding higher multiplicity.*

Proof. The field of tangent planes to the limit shape is the family of planes $\{x_3 - sx - ty - c = 0 \mid u \in \mathbb{H}\}$ where x_3 denotes the third coordinate, and $s = s(z), t = t(z), c = c(u)$ with $z = z(u)$ rational as above. The limit shape surface is defined as the envelope of these planes, that is, as the solution to the simultaneous system

$$\begin{aligned} x_3 &= sx + ty + c \\ 0 &= s_u x + t_u y + c_u. \end{aligned}$$

The second equation here is complex and thus gives two real (and linear) relations on x, y . At a critical point of z , $s_u = \frac{ds}{dz} \frac{dz}{du} = 0$ and likewise $t_u = \frac{dt}{dz} \frac{dz}{du} = 0$. So there is a finite value of (x, y) only if $c_u = 0$ at this point as well. Likewise for higher multiplicity. \square

What remains is to find the parameters a_i so that c satisfies the condition of Lemma 2.1 and the values of s_u, t_u, c_u at a_1, a_2, \dots, a_{4n} in (4) match the lines of the corresponding sides of R_0 . To carry this out in practice it seems unavoidable to have to solve an algebraic system of equations; however existence and uniqueness of the limit shape imply that there is a unique solution for which the a_i are cyclically ordered clockwise on $\hat{\mathbb{R}}$. We illustrate the method with the two easiest cases of $n = 1$ and $n = 2$ in the next sections.

2.1 Aztec diamond

The simplest case is when $n = 1$ and thus R_0 is a square; this is the case of the Aztec diamond, first defined in [9]. See Figure 3. In this case we can take $z = u$, since the cover is of degree 1. The s, t, c functions as functions of z for $z \in \mathbb{R}$ are (in blue in the figure):

	$-1 < z < 0$	$0 < z < 1$	$1 < z < \infty$	$-\infty < z < -1$
	$0 > w > -1$	$-1 > w > -\infty$	$\infty > w > 1$	$1 > w > 0$
s	0	1	1	0
t	0	0	1	1
c	0	0	-1	0

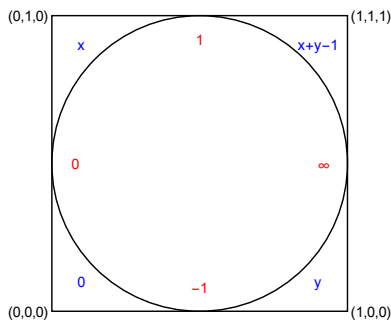


Figure 3: Aztec diamond with z values in red and boundary tangent planes in blue (the blue quantities are the linear equations for the facets: for example the upper right facet lies in the plane $x_3 = x + y - 1$). The quantities s, t, c for each facet are the coefficient of x , the coefficient of y , and the constant term, respectively. Vertices of the outer polygon are labeled with their coordinates in \mathbb{R}^3 (the third coordinate being the height function).

Since c is harmonic in $z \in \mathbb{H}$ it is defined from its boundary values

$$c = \frac{-\pi + \text{Arg}(z - 1)}{\pi}.$$

The s, t values are also harmonic; notice that they satisfy (3).

In this case there is no condition from Lemma 2.1. The surface can be found as the envelope of the planes $x_3 = sx + ty + c$ as z varies over \mathbb{H} . We can find $x, y, h = x_3$ as a function of z by solving the simultaneous linear equations (with coefficients which are functions of z) for h, x, y :

$$\begin{aligned} sx + ty + c &= h \\ s_z x + t_z y + c_z &= 0 \\ s_{\bar{z}} x + t_{\bar{z}} y + c_{\bar{z}} &= 0 \end{aligned} \tag{5}$$

Here the third equation is redundant as it follows from the second one, however it is useful to record for computational purposes. Solving equations (5) we find

$$(x, y) = \left(\frac{|z|^2}{1 + |z|^2}, \frac{|z + 1|^2}{2(1 + |z|^2)} \right),$$

and

$$h = -1 + \frac{\text{Arg}(z - 1)}{\pi} + \frac{|z|^2(\pi - \text{Arg}(z))}{\pi(1 + |z|^2)} + \frac{|z + 1|^2(\pi + \text{Arg}(z))}{2\pi(1 + |z|^2)}.$$

See Figure 4. This Aztec diamond example was treated with the same method in Section 6.1 of [15], but with a different convention for the Newton polygon N .

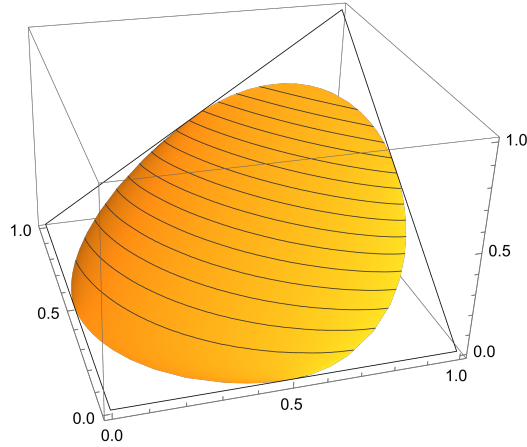


Figure 4: Aztec diamond limit shape surface with contour lines for the height function (the vertical axis is the height function). (Shown is the rough phase region; the limit shape is linear on each component outside the rough phase region.)

2.2 Symmetric octagon

Suppose R_0 is the octagon of Figure 5 which has a reflection symmetry along the line $x = y$. (This symmetry is not essential for the theory but makes the calculations easier.)

We have 8 parameters a_1, \dots, a_8 . We have the freedom of a Möbius transformation to set $a_1 = 0, a_2 = -1, a_8 = \infty$. By symmetry of R_0 , we then necessarily have $a_i = \rho/a_{9-i}$ for some ρ to be determined as a function of the edge lengths m_1, m_2 . Set $z = B_1 \frac{(u-a_4)}{(u+1)(u-a_6)}$. Then the fact that $z = -1$ at $u = 0$ determines B_1 to be $B_1 = a_6/a_4$. Likewise $z = -1$ at $u = a_5 = \rho/a_4$ determines ρ as a function of a_4, a_6 : $\rho = a_4 a_6 - a_4 + a_6$.

The functions s, t, c are determined in terms of the remaining two variables a_4, a_6 by the following table of their boundary values.

u	$(-\infty, a_7)$	(a_7, a_6)	(a_6, a_5)	(a_5, a_4)	(a_4, a_3)	(a_3, a_2)	(a_2, a_1)	(a_1, ∞)
z	$(0, 1)$	$(1, \infty)$	$(\infty, -1)$	$(-1, 0)$	$(0, 1)$	$(1, \infty)$	$(\infty, -1)$	$(-1, 0)$
s	1	1	0	0	1	1	0	0
t	0	1	1	0	0	1	1	0
c	0	-1	$m_1 - 1$	$m_1 - m_2$	$m_1 - 1$	-1	0	0

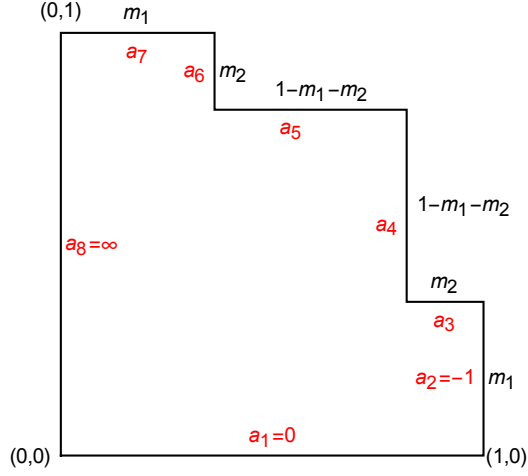


Figure 5: An octagon with diagonal symmetry, with u values at tangency points marked in red.

For example

$$c = \frac{1}{\pi} \left(-\arg\left(\frac{u-a_6}{u-a_7}\right) + (m_1-1)\arg\left(\frac{u-a_5}{u-a_6}\right) + (m_1-m_2)\arg\left(\frac{u-a_4}{u-a_5}\right) + (m_1-1)\arg\left(\frac{u-a_3}{u-a_4}\right) - \arg\left(\frac{u-a_2}{u-a_3}\right) \right).$$

A short calculation shows that c_u vanishes at the critical points of z if

$$a_6 = \frac{2 - m_1 - m_2}{m_2 - m_1}.$$

Then the fact that $z = 1$ at $a_7 = \rho/a_2$ determines a_4 :

$$a_4 = -\frac{(\sqrt{2}+1)(2-m_1-m_2)}{2(1-m_2)}.$$

We thus have $(a_1, \dots, a_8) =$

$$= \left(0, -1, -\sqrt{2}, -\frac{(1+\sqrt{2})(2-m_1-m_2)}{2(1-m_2)}, -\frac{(4-2\sqrt{2})(1-m_2)}{m_1-m_2}, -\frac{2-m_1-m_2}{m_1-m_2}, -\frac{\sqrt{2}(2-m_1-m_2)}{m_1-m_2}, \infty \right). \quad (6)$$

This leads to the limit shape of Figure 6.

There is a nontrivial inequality on m_1, m_2 in order for R_0 to be feasible (that is, in order for there to exist a tiling): this feasibility is equivalent to (a_1, \dots, a_8) of (6) being in the correct (cyclic) order on $\hat{\mathbb{R}}$. We need

$$m_1 \geq m_2 \geq (3 + 2\sqrt{2})m_1 - 2(1 + \sqrt{2}).$$

See Figure 7 for arctic curves near the two edges of the parameter space.

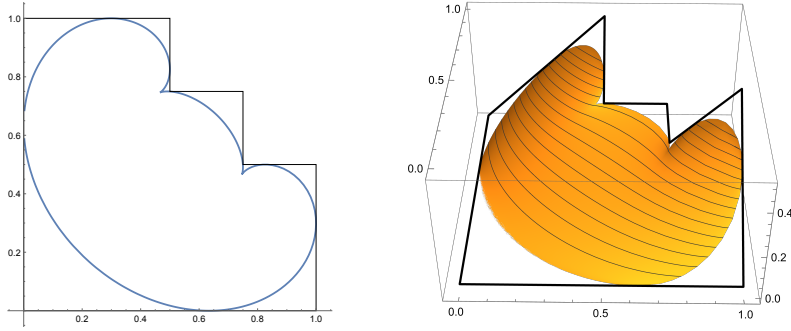


Figure 6: Domino arctic curve and rough phase region limit shape when $m_1 = \frac{1}{2}, m_2 = \frac{1}{4}$.

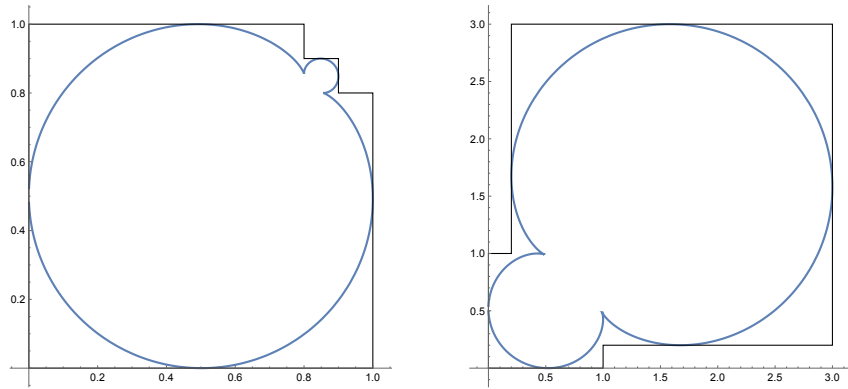


Figure 7: Domino arctic curves when $m_1 = \frac{4}{5}, m_2 = \frac{1}{10}$ and when $m_1 = \frac{1}{5}, m_2 = -2$.

2.3 Aztec fortress

We consider the square-octagon lattice dimer model with weights $1, a$ on edges as shown in Figure 8. This dimer model is equivalent to the square lattice dimer model with 2-periodic weights, as shown in Figure 8.

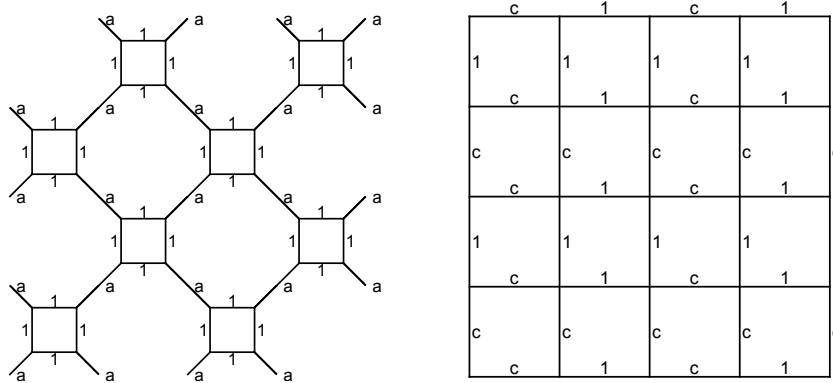


Figure 8: Square-octagon lattice and two-periodic square lattice. There is a weight-preserving correspondence between dimers on these two lattices if $2c = a^2$, see [17].

The Newton polygon for either of these lattices is

$$N = cvx\{(1, 0), (0, 1), (-1, 0), (0, -1)\}.$$

The surface tension σ is strictly convex in the interior of N , and analytic in N except for a conical singularity at $(0, 0)$ (when $c \neq 1$). Here z , the conformal coordinate, is parameterized by an annulus which we choose to be $\mathbb{A} = [0, 2] \times [0, \tau]/\sim$ where \sim identifies the right and left boundaries by translation, with $\tau = \tau(c)$.

The ‘‘Aztec fortress’’ boundary conditions [17] for the square octagon lattice are equivalent to the Aztec diamond boundary conditions for the square grid dimer model with the above 2-periodic weights. For these boundary conditions we can take $z = u$: the rough phase region maps to the annulus with degree 1. The lower boundary of the annulus \mathbb{A} corresponds to the outer arctic boundary, and the upper boundary of \mathbb{A} corresponds to the inner (‘‘smooth/rough’’) boundary.

Using the 4-fold symmetry, the function s has values $1, 0, -1, 0$ on the lower boundary of \mathbb{A} for z respectively in the intervals $[0, 1/2], [1/2, 1], [1, 3/2], [3/2, 2]$, and value 0 in the upper boundary. The harmonic extension of these boundary values allows s to be written explicitly in terms of elliptic functions. It is convenient to use the Weierstrass σ -function (defined in e.g. [1], not to be confused with the surface tension). With $\tau = 1$ we have

$$s(z) = 1 - \frac{\text{Im}(z)}{2} - \frac{1}{\pi} \arg \frac{\sigma(z)\sigma(z + \frac{1}{2})}{\sigma(z+1)\sigma(z + \frac{3}{2})},$$

and likewise

$$t(z) = \frac{1}{\pi} \arg \frac{\sigma(z - \frac{1}{2})\sigma(z - 2)}{\sigma(z - 1)\sigma(z - \frac{3}{2})},$$

$$c(z) = 1 - \frac{\text{Im}(z)}{2} + \frac{2}{\pi} \arg \frac{\sigma(z)\sigma(z + \frac{1}{2})}{\sigma(z + 1)\sigma(z + \frac{3}{2})}.$$

These expressions can be checked by differentiation, using $\frac{d}{dz} \log \sigma(z) = \zeta(z)$, where ζ is the Weierstrass zeta function, the analog of “ $1/z$ ” on the associated torus. The limit shape for $\tau = 1$ is shown in Figure 9.

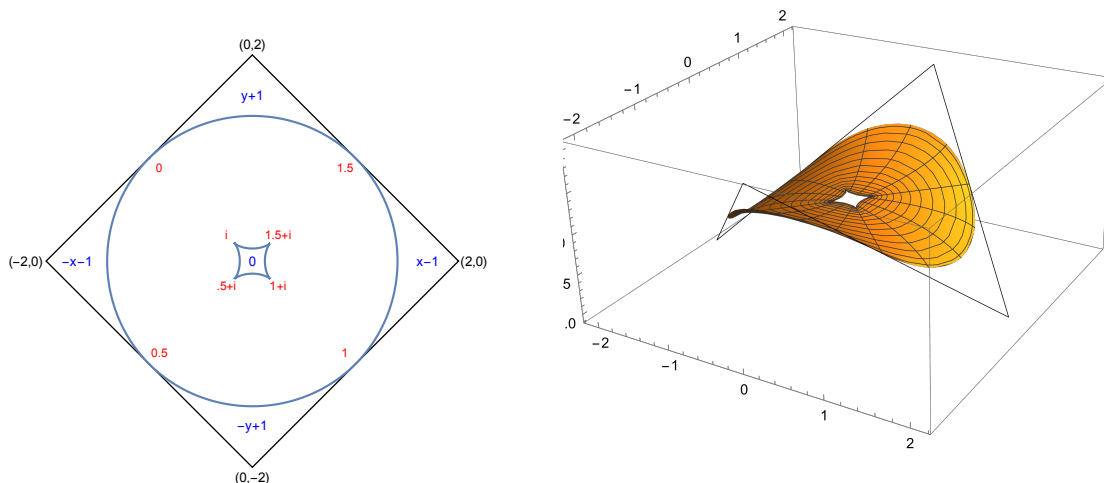


Figure 9: For the square-octagon dimer model on a “fortress” region, the arctic curve with facet equations (left) and 3d rough phase region limit shape (right).

3 Five vertex model

The five vertex model [8, 14] is a model of non-intersecting north- and west-going lattice paths in \mathbb{Z}^2 . The probability of a configuration (on a finite domain) is proportional to the product of its vertex weights as given in Figure 10. Here $1 < r < \infty$ is a parameter².

The features of the 5-vertex model which are relevant for the current discussion are as follows.

²One can also define and solve the model for $0 < r < 1$, setting the weight of the empty vertex to be $1 - r^2$, see [8, 14]. We will not consider this case here.

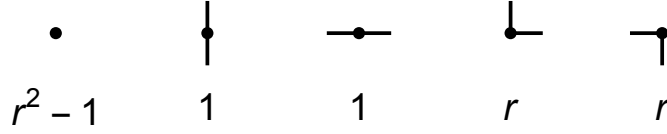


Figure 10: Vertex weights for the 5-vertex model.

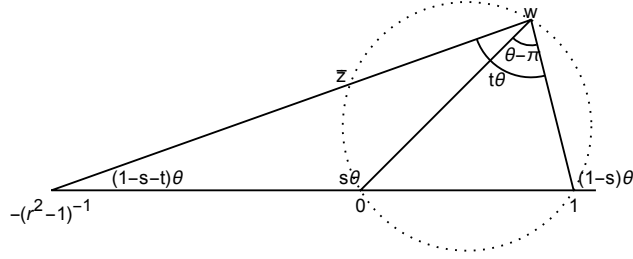


Figure 11: Relationship between r, s, t, w, z, θ in the 5-vertex model. Given r, w we can draw a circle passing through $0, 1, w$. Then z, θ, s, t are determined as shown.

1. Let $N = \text{conv}\{(0, 0), (1, 0), (0, 1)\}$; the surface tension $\sigma = \sigma(s, t)$ is strictly convex and analytic on the interior of N and $+\infty$ outside of N .
2. The intrinsic coordinate z can be chosen to be parameterized by $z \in \bar{\mathbb{H}}$. There is another intrinsic coordinate w , where $w \in \mathbb{H}$, related to z through the spectral curve $P(z, w) = 1 - z - w + (1 - r^2)zw = 0$.
3. For $(s, t) \in N$ we have $t(z) = \frac{\pi + \text{Arg} z}{\theta}$ and $s(z) = t(\bar{w}) = \frac{\pi - \text{Arg} w}{\theta}$ where $\theta(z) = 2\pi + \text{Arg} \frac{z}{1-z} = 2\pi - \text{Arg} \frac{w}{1-w}$. See Figure 11.

The five vertex model limit shape is the envelope of the family of planes parameterized by $u \in \mathbb{H}$ (we use x_3 for the third coordinate)

$$x_3 = sx + ty + c. \quad (7)$$

The surface itself is the envelope of these planes; it is obtained by solving simultaneously both (7) and its derivative which is (see [14, Corollary 4.3])

$$x_3 = \frac{(\theta s)_u}{\theta_u} x + \frac{(\theta t)_u}{\theta_u} y + \frac{(\theta c)_u}{\theta_u} \quad (8)$$

where $z = z(u)$ is an appropriate holomorphic map. Since $\theta, \theta s, \theta t$ and θc are harmonic, they can be determined from their boundary values, that is, for $u \in \mathbb{R}$: see a worked example in the next section.

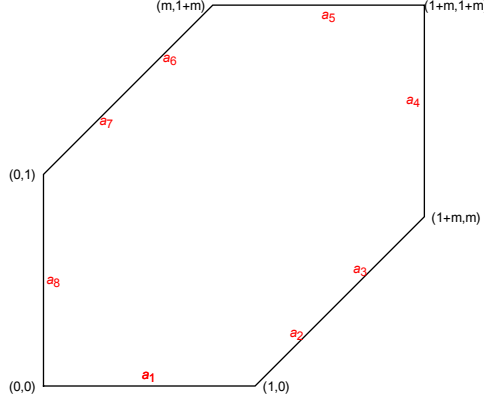


Figure 12:

3.1 5-vertex boxed plane partition

Here we determine the limit shape for the 5-vertex model in a hexagon. See Figure 12. This limit shape was first determined in [8] by a different method; the method presented here leads to a more explicit form of the limit shape and is more amenable to generalizations. We parametrize the rough phase region by $u \in \bar{\mathbb{H}}$ (via an orientation-preserving diffeomorphism in this case), and $z(u) \in \bar{\mathbb{H}}$ is a degree-2 cover, to be determined. There are 8 tangency points to R_0 of the arctic curve, where u takes real values a_1, \dots, a_8 . We set $a_8 = \infty, a_1 = 0$, and order them as $a_7 \leq a_6 \leq \dots \leq a_1 = 0$. We determine the intercept function $c = c(u)$ as follows. Recall that $c(u)$ is a ratio of two harmonic functions, $c(u) = \frac{G(u)}{\theta(u)}$. The boundary values of c and θ are determined from the following table, which allows us to find the boundary values of G . The harmonicity of G allows us to define $G(u)$ in all of \mathbb{H} , from which we get $c(u)$.

u	$(-\infty, a_7)$	(a_7, a_6)	(a_6, a_5)	(a_5, a_4)	(a_4, a_3)	(a_3, a_2)	(a_2, a_1)	(a_1, ∞)
z	$(-1, 0)$	$(0, 1)$	$(1, \infty)$	$(-\infty, -1)$	$(-1, 0)$	$(0, 1)$	$(1, \infty)$	$(-\infty, -1)$
s	1	1/2	0	0	1	1/2	0	0
t	0	1/2	1	0	0	1/2	1	0
c	0	-1/2	-1	m	-1	-1/2	0	0
θ	π	2π	π	π	π	2π	π	π
$\frac{G}{\pi}$	0	-1	-1	m	-1	-1	0	0

This gives

$$G = -\arg\left(\frac{u - a_7}{u - a_6}\right) - \arg\left(\frac{u - a_6}{u - a_5}\right) + m \arg\left(\frac{u - a_5}{u - a_4}\right) - \arg\left(\frac{u - a_4}{u - a_3}\right) - \arg\left(\frac{u - a_3}{u - a_2}\right).$$

Using symmetry along the major diagonal we set $a_5 = 1/a_4, a_6 = 1/a_3, a_7 = 1/a_2$. Symmetry along the minor diagonal then relates the a s under the map $u \mapsto \frac{u - a_4}{a_4 u - 1}$. This gives $a_3 = \frac{a_2 - a_4}{a_2 a_4 - 1}$, and there are two remaining parameters a_2, a_4 .

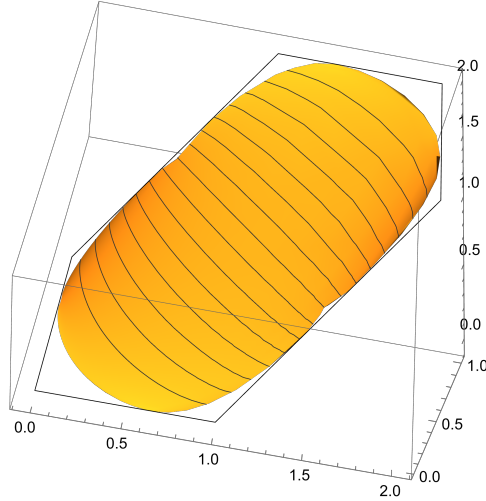


Figure 13: The 5-vertex model with “boxed plane partition” boundary conditions, showing height contours, with $r = \sqrt{2}$, $m = 1$. Observe the small facets in the middle of the diagonal edges (pictured in white).

We have $z = B \frac{(u-a_3)(u-a_7)}{u(u-a_5)}$ and $B = -1$ by setting $u = \infty$. Also $1 = z(a_2)$ sets one of the remaining parameters. The last parameter is determined by $G'(u) = 0$ when $z'(u) = 0$. This leads to

$$(a_1, \dots, a_4) = \left(0, -\frac{\sqrt{m}}{2^{1/4}\sqrt{m+2}}, -\frac{2^{1/4}\sqrt{m}}{\sqrt{m+2}}, -\frac{2 + \sqrt{2}}{2^{7/4}} \frac{\sqrt{m(m+2)}}{m+1} \right)$$

and (a_8, a_7, a_6, a_5) are inverses of these. This leads to the limit shape of Figure 13.

4 Four-vertex model versus lozenge tilings

In this section, we consider the four-vertex model which is a degenerate case of the five-vertex model, where the third type of vertex in Figure 10 has weight 0. Its arctic curves for specific (analogous to boxed plane partition) boundary conditions were recently studied in [6]. In order to be consistent with [6] we also switch to north- and east-going lattice paths in this discussion, i.e. mirror the last two configurations with respect to the vertical axis in Figure 10. We find that limit shapes of the four-vertex model, viewed as surfaces in three dimensions, are, after a certain fixed linear transformation, lozenge tiling limit shapes. The linear transformation in our setup is a shearing transformation of the form

$$(x, y, h) \mapsto (x, y - x - h, h.) \tag{9}$$

This follows from a simple bijection on the level of configurations: see Figure 14.

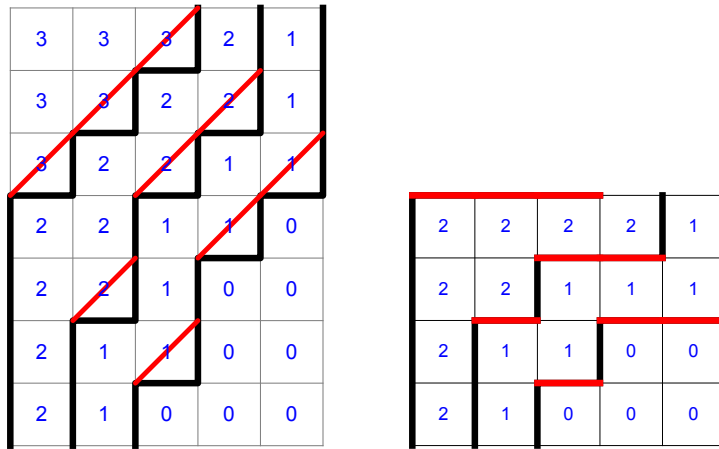


Figure 14: Left: a 4-vertex configuration in black, with height function on faces. Each horizontal black edge has a vertical edge immediately to its right; join these with a diagonal edge as shown (red). Then applying a linear map $(x, y, h) \rightarrow (x, y - x - h, h)$, the images of the vertical black edges and diagonal red edges form a standard monotone non-intersecting NE lattice path configuration (right), or equivalently, a lozenge tiling configuration. Each red segment replaces two corners in 4-vertex model; therefore giving a red segment a weight r^2 , this becomes a weight-preserving bijection from $4V$ to lozenges with weight 1 for vertical edges and r^2 for horizontal edges (and $r^2 - 1$ for empty vertices).

From the five-vertex degeneration point of view, one would expect the surface tension of the four-vertex model to satisfy the trivial potential property. This is indeed the case which we explain below. We find it interesting that a simple linear transform leads to a trivial potential property.

Our conventions for the height functions, see Figure 14, induces the Newton polygons

$$\tilde{N} = \text{conv}\{(0, 0), (-1, 0), (-1/2, 1/2)\} \quad \text{and} \quad N = \text{conv}\{(0, 0), (-1, 0), (0, 1)\}$$

for the four-vertex model (left side) and a lozenge tiling model (right side), respectively.

Let σ be the surface tension of the lozenge model. This has a representation in terms of the intrinsic $z \in \mathbb{H}$ with harmonic functions $s(z), t(z)$ and $X(z), Y(z)$ such that

$$X_z + i\pi t_z = 0 \quad Y_z - i\pi s_z = 0, \tag{10}$$

and the correspondence $\nabla\sigma(s, t) = (X, Y)$, see [15]. The Legendre dual of σ , the free energy, is denoted by $F(X, Y)$. Its graph $(X, Y, F(X, Y))$ describes the corresponding Wulff shape in \mathbb{R}^3 . Because of the above correspondence (9), the Wulff shape of the 4-vertex model is also a three dimensional shearing of the lozenge tiling Wulff shape, by considering the inverse:

$$(X, Y, F) \mapsto (\tilde{X}, \tilde{Y}, \tilde{F}) = (X, Y + X + F, F) \tag{11}$$

We record next the effect of this linear change on the surface tension. The relevant transformation between the Newton polygons $N \rightarrow \tilde{N}$ is

$$(s, t) \mapsto (\tilde{s}, \tilde{t}) = \left(\frac{s-t}{1+t}, \frac{t}{1+t} \right)$$

The surface tension $\tilde{\sigma}$ of the 4-vertex model is

$$\tilde{\sigma}(\tilde{s}, \tilde{t}) = (1 - \tilde{t}) \sigma\left(\frac{\tilde{s} + \tilde{t}}{1 - \tilde{t}}, \frac{\tilde{t}}{1 - \tilde{t}}\right) = \frac{\sigma(s, t)}{1 + t}.$$

Indeed, by a direct calculation one verifies that

$$\tilde{\sigma}_{\tilde{s}}(\tilde{s}, \tilde{t}) = \sigma_s(s, t) = X \quad \text{and} \quad \tilde{\sigma}_{\tilde{t}}(\tilde{s}, \tilde{t}) = Y + X + F(X, Y).$$

The same variable $z \in \mathbb{H}$ parametrises both the slopes (\tilde{s}, \tilde{t}) and the external fields (\tilde{X}, \tilde{Y}) , by the indicated change of variables. We now verify that z is an intrinsic coordinate and the model has a trivial potential. We find that

$$\tilde{X}_z + i\pi(1+t)^2\tilde{t}_z = X_z + i\pi t_z = 0,$$

and (using $F_z = F_X X_z + F_Y Y_z = sX_z + tY_z$)

$$\tilde{Y}_z - i\pi(1+t)^2\tilde{s}_z = (1+t)(Y_z - i\pi s_z) + (1+s)(X_z + i\pi t_z) = 0,$$

because of (10). This means by Proposition 2.1 of [15] that z is an intrinsic coordinate for $\tilde{\sigma}$ and $\kappa(z) = \sqrt{\det H_{\tilde{\sigma}}} = \pi(1+t)^2$. Furthermore, since $\kappa^{1/2}(z) = \sqrt{\pi}(1+t(z))$ is a harmonic function, $\tilde{\sigma}$ has a trivial potential.

In fact, we observe that the surface tension $\tilde{\sigma}$ has the same structure as the general large r 5-vertex model (see Theorem 3.2 b of [14]): the boundary values of $\sqrt{\det H_{\tilde{\sigma}}}$ are equal to π in the corners $(0,0)$ and $(-1,0)$ and 4π in the corner $(-1/2,1/2)$, and the extension inside is dictated by the harmonicity of $\kappa^{1/2}(z)$. The behaviours at these two types of corners are referred to as ferroelectric and anti-ferroelectric phases in [6].

Remark 1. *In the example of [6], for the so-called ‘scalar-product’ boundary conditions, the arctic curve is found to be consisting of six arcs, each of them is a portion of certain ellipses. This can be explained via the reduction to lozenge model, as follows. It is easily seen that the transformation (9) deforms the scalar-product boundary conditions to hexagonal (or ‘boxed plane-partition’) boundary conditions for the lozenge model. Its well-known arctic curve is the inscribed ellipse to the hexagon. Note that the height function h is affine on each six arcs of the ellipse between tangency points. Thus when we move back to the 4-vertex setting with the inverse of (9)*

$$(x, y) \mapsto (x, y + x + h),$$

the single ellipse is transformed to six different ellipses depending on the behaviour of h . Note, however, that the arctic curves viewed as curves in three dimensions are related by a single linear transformation. Only when projected to the (x, y) -plane do the six different linear transformations become apparent.

Acknowledgements. IP is grateful to the Workshop on ‘Randomness, Integrability, and Universality’, held in Spring 2022 at the Galileo Galilei Institute for Theoretical Physics, as well as to Yale University for hospitality during his visit in December 2022. RK thanks the University of Helsinki for a visit in summer 2023 where some of this research was performed. We acknowledge Benoît Laslier for a simultaneous observation about the linear relationship between 4-vertex and lozenge limit shapes. We thank the anonymous referees for their valuable comments.

References

- [1] Lars Ahlfors. *Complex analysis—an introduction to the theory of analytic functions of one complex variable*. AMS Chelsea Publishing, Providence, RI, third edition, 2021.
- [2] Kari Astala, Erik Duse, István Prause, and Xiao Zhong. Dimer models and conformal structures, 2020, arXiv:2004.02599.
- [3] Kari Astala, Tadeusz Iwaniec, and Gaven Martin. *Elliptic partial differential equations and quasiconformal mappings in the plane*, volume 48 of *Princeton Mathematical Series*. Princeton University Press, Princeton, NJ, 2009.

- [4] Tomas Berggren and Alexei Borodin. Geometry of the doubly periodic aztec dimer model, 2023, arXiv:2306.07482.
- [5] Yannis Brun and Jérôme Dubail. The Inhomogeneous Gaussian Free Field, with application to ground state correlations of trapped 1d Bose gases. *SciPost Phys.*, 4:37, 2018.
- [6] I. N. Burennev, F. Colomo, A. Maroncelli, and A. G. Pronko. Arctic curves of the four-vertex model, 2023, arXiv:2307.03076.
- [7] Henry Cohn, Richard Kenyon, and James Propp. A variational principle for domino tilings. *J. Amer. Math. Soc.*, 14(2):297–346, 2001.
- [8] Jan de Gier, Richard Kenyon, and Samuel S. Watson. Limit shapes for the asymmetric five vertex model. *Comm. Math. Phys.*, 385(2):793–836, 2021.
- [9] Noam Elkies, Greg Kuperberg, Michael Larsen, and James Propp. Alternating-sign matrices and domino tilings. I. *J. Algebraic Combin.*, 1(2):111–132, 1992.
- [10] R. Kenyon. The Laplacian and Dirac operators on critical planar graphs. *Invent. Math.*, 150(2):409–439, 2002.
- [11] Richard Kenyon. Lectures on dimers. In *Statistical mechanics*, volume 16 of *IAS/Park City Math. Ser.*, pages 191–230. Amer. Math. Soc., Providence, RI, 2009.
- [12] Richard Kenyon and Andrei Okounkov. Limit shapes and the complex burgers equation. *Acta Mathematica*, 199(2):263–302, 2007.
- [13] Richard Kenyon, Andrei Okounkov, and Scott Sheffield. Dimers and amoebae. *Annals of Mathematics*, pages 1019–1056, 2006.
- [14] Richard Kenyon and István Prause. The genus-zero five-vertex model. *Probab. Math. Phys.*, 3(4):707–729, 2022.
- [15] Richard Kenyon and István Prause. Gradient variational problems in \mathbb{R}^2 . *Duke Math. J.*, 171(14):3003–3022, 2022.
- [16] K. Palamarchuk and N. Reshetikhin. The 6-vertex model with fixed boundary conditions, 2010, arXiv:1010.5011.
- [17] James Propp. Generalized domino-shuffling. *Theoretical Computer Science*, 303(2):267–301, 2003. Tilings of the Plane.